Front. Phys. China, 2009, 4(3): 356–366
DOI 10.1007/s11467-009-0050-6

REVIEW ARTICLE

Hydrogen adsorption and desorption on the Pt and Pd subnano clusters – a review

Liang CHEN (陈亮)[1], **Cheng-gang ZHOU** (周成冈)[2], **Jin-ping WU** (吴金平)[2], **Han-song CHENG** (程寒松)[2]

[1] *Ningbo Institute of Materials Technology and Engineering, Chinese Academy of Sciences, Ningbo 315201, China*
[2] *Institute of Theoretical Chemistry and Computational Materials Science, China University of Geosciences, Wuhan 430074, China*
[3] *Air Products and Chemicals, Inc. 7201 Hamilton Boulevard, Allentown, PA 18195, USA*
E-mail: chenliang@nimte.ac.cn

Received January 24, 2009; accepted March 12, 2009

In this review, we present our recent first principles studies on the sequential H_2 dissociative chemisorption and H desorption on the Pt_n and Pd_n clusters (n=2−9, 13). Upon full saturation by H atoms, the calculated H_2 dissociative chemisorption energy and H desorption energy on Pt_{13} and Pd_{13} clusters are similar to the corresponding values on smaller close-packed clusters. Indeed, the catalytic performances of these subnano clusters do not vary significantly with the particle sizes or shapes. Instead, they are dependent on the surface metal atoms which can be accessed by H atoms. In addition to the coverage dependency of the H_2dissociative chemisorption and H sequential desorption energies, the phase transition of both Pt_{13} and $Pd_{13}$from the icosahedral to *fcc*-like structures at certain H coverage was also investigated.

Keywords hydrogen adsorption, density functional theory, metal clusters, catalysis

PACS numbers 68.43.Bc, 68.47.Jn, 71.15.Mb, 82.65.+r

Contents

1 Introduction

Hydrogen dissociative chemisorption on transition metal catalysts is of great industrial interest in many applications such as hydrogenation, hydrogen storage and electrocatalysis [1−6]. In the past few decades, a great deal of experimental and theoretical efforts have been made to understand the mechanisms of the catalytic processes on Pt, Pd and other precious transition metal surfaces in order to develop low-cost and efficient catalysts for hydrogenation [7−12]. For example, some studies using thermal desorption spectroscopy reported that the dissociative chemisorption energy of hydrogen on the Pt(111) surface is between 0.70 and 0.83 eV [13, 14]. Accordingly, many theoretical studies have employed single crystalline surface models at low coverage of H_2 to represent catalyst surfaces [12, 15, 16]. The reported dissociative chemisorption energy of hydrogen on these Pt crystalline surfaces ranges from 0.8 to 1.54 eV. On the other hand, Watson and coworkers have calculated the adsorption and thermally activated diffusion of hydrogen on the Pd(111) surface with the variation of adsorption sites at low H coverage [17]. They found that the *fcc* hollow site with an adsorption energy of 0.53 eV is the most favorable site. Nobuhara investigated the low coverage dependency of hydrogen absorption into Pd(111) and the corresponding variation in the energy barrier for

H absorption [18, 19].

However, in a realistic catalytic system, the Pt and Pd catalysts are usually dispersed on the support materials in the form of particles (or clusters) with different sizes and shapes. The dissociative chemisorption and desorption behaviors of hydrogen on such particles and perfect crystalline surfaces should be significantly different due to the fact that finite-size particles possess sharp corners and edges, which are usually the most active sites for catalytic reactions [20−22]. A recent desorption experiment of hydrogen/deuterium on a Pt_{13} cluster supported by NaY zeolite yielded an H_2 dissociative chemisorption energy of 1.36 eV [23], which is much higher than on single crystalline surfaces. Using density functional theory (DFT) methods, Okamoto also reported a similar chemisorption energy of 1.4 eV for H_2 dissociative adsorption at the on-top sites of a Pt_{13} cluster [24, 25]. These results clearly demonstrate that the chemical reactivity of H_2 on clusters is much higher than on crystalline surfaces. Furthermore, several calculations also suggested substantially higher desorption energy for atomic hydrogen adsorbed on clusters than on flat crystalline surfaces. For example, the desorption energy of an H atom on the Pt(111) surface was found to be 2.60−2.65 eV [26−28]. In contrast, Watari reported a H desorption energy of 2.9−4.5 eV on a Pt_{13} cluster [29].

Recently, Cheng and coworkers reported strong coverage dependency of catalytic activity of Pt and Pd clusters [30−32]. The dissociative chemisorption energy of H_2 on these catalyst surfaces at low coverages is considerably higher than at high coverages. In a typical hydrogenation reaction, a certain pressure of hydrogen is always maintained and the catalyst particles should be fully covered by either molecular or atomic hydrogen, consequently their catalytic performance is also expected to be coverage dependent. Indeed, much insight into the catalytic activity using low H coverage and single crystalline surface models has already been obtained. However, to more adequately address the realistic catalytic activity, it is very critical to understand the chemical behaviors of the Pt and Pd clusters that are saturated by H atoms to simulate the real catalytic environment. Unfortunately, comprehensive modeling of realistic particle size of catalysts using first principles methods would be computationally difficult since the calculations would involve a very large number of atoms.

In this review, we present our recent first principles studies on the sequential hydrogen chemisorption on a series of subnano Pt_n and Pd_n clusters (n=2−9, 13) to address their catalytic activity [30−33]. We show that at full H-saturation the H_2 dissociative chemisorption energy and the H desorption energy on those clusters do not change significantly with the cluster sizes and shapes. This review is aimed at enhancing our understanding of the interplay between hydrogen and Pt/Pd subnano clusters at or near full H coverage. The literatures on hydrogen sorption on Pt and Pd catalysts at low coverages have been reviewed and discussed by many authors [9, 12, 17, 33], which will not be focused on in this review.

2 Models and computational details

Our calculations were carried out using DFT methods with the Perdew–Wang exchange-correlation functional and a spin-polarized scheme [34]. The effective core pseudopotential (ECP) was utilized to describe the core electrons and a double numerical basis set augmented with polarization function (DNP) was employed to describe the valence electrons. The energy and gradient convergence tolerance was chosen to be 2×10^{-5} Ha and 4×10^{-3} Ha/Å, respectively. All structures are fully optimized using conjugated gradient algorithm without symmetry constrains. We also employed the LST/QST method to identify the transition state of H_2 dissociative chemisorption and diffusion on the Pt and Pd clusters [35]. The NVT molecular dynamics (MD) simulations and bond-distance distribution analysis were performed to investigate the structural rearrangement and identify the hydrogen saturation point. The Hirshfeld population analysis was performed to evaluate the charge transfer from metal clusters to hydrogen [36]. All computational methods were implemented in $DMol^3$ package [37, 38].

The H_2 dissociative chemisorption energy ΔE_{CE} and the H sequential desorption energy ΔE_{DE} are defined as follows:

$$\Delta E_{\mathrm{CE}} = -\frac{2}{x}\left(E_{\mathrm{P}_n\mathrm{H}_x} - E_{\mathrm{P}_n} - \frac{x}{2}E_{\mathrm{H}_2}\right) \quad (1)$$

$$\Delta E_{\mathrm{DE}} = E_{\mathrm{H}} - \frac{1}{2}(E_{\mathrm{P}_n\mathrm{H}_x} - E_{\mathrm{P}_n\mathrm{H}_{x-2}}) \quad (2)$$

where n is the number of H atoms. $E_{\mathrm{P}_n\mathrm{H}_x}$ is the energy of P_nH_x hydrides, E_{P_n} is the energy of bare metal clusters and E_{H_2} is the energy of a H_2 molecule.

For Pt and Pd, the growth path from a few atoms to a bulk may adopt three patterns, i.e., the close-packed triangular pattern, the icosahedral pattern and the *fcc*-like pattern. In our recent studies, we found that at the subnano scale, both Pt and Pd clusters initially adopt a close-packed triangular growth pattern, followed by an abrupt transition to the icosahedral growth pattern at a certain point [39]. Therefore, we selected close-packed structures for smaller Pt_n and Pd_n (n = 2–9) clusters, which are taken directly from our previous reports [39]. For larger Pt_{13} and Pd_{13} cluster, we selected the smallest icosahedral cluster as a model.

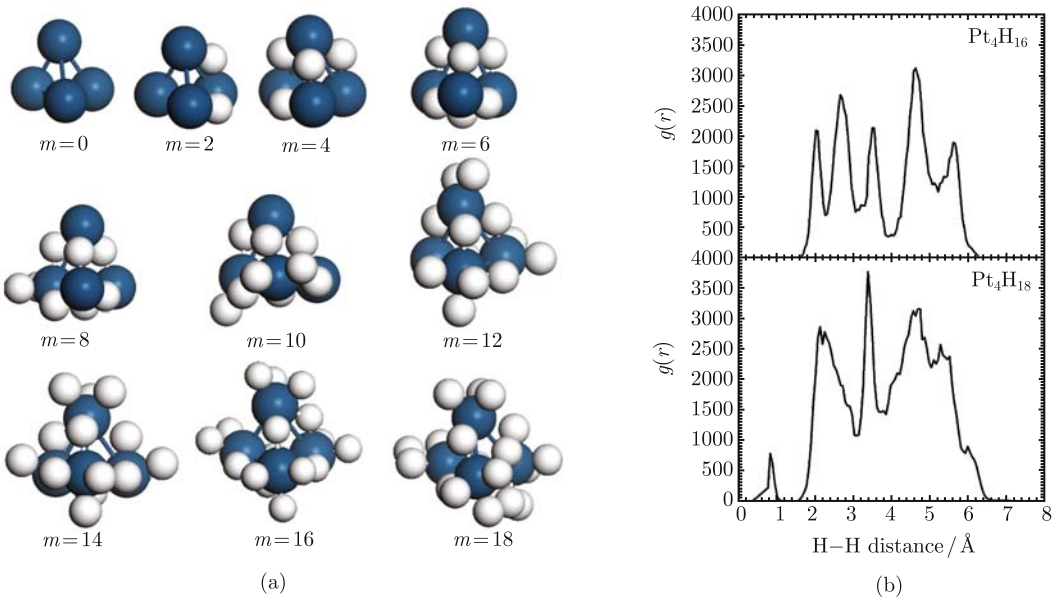

Fig. 1 **(a)** Optimized structures of H_2 sequential dissociative chemisorption on a Pt_4 cluster and **(b)** The calculated H–H distance distributions for Pt_4H_{16} and Pt_4H_{18}, respectively. Reprinted with permission from Ref. [31]. Copyright © 2007 American Chemical Society.

3 Results and discussion

3.1 Hydrogen chemisorption on close-packed Pt_n clusters (n = 2–9)

We first investigated the chemisorption on the small close-packed Pt_n clusters (n = 2–9). For convenience, we choose the Pt_4 cluster as an example to show the sequential H_2 dissociative chemisorption process. On the Pt_4 tetrahedron, there are three possible adsorption sites available for H adsorption: one-fold on-top, two-fold edge and three-fold hollow site. The on-top site is identified as energetically the most favorable binding site, followed by the edge site. Figure 1(a) displays the fully optimized Pt_4 structures at varying H coverages. Depending on the coverage, the cluster is distorted to a certain extent. Full saturation is reached when 16 H atoms are adsorbed, while excessive H adsorption would result in recombination of H atoms to form H_2 molecules. In fact, upon loading 18 H atoms on the cluster, the trajectories of MD simulations for up to 2 ps show that two H atoms are readily squeezed out of the cluster, forming a H_2 molecule which subsequently desorbs to the gas phase. Indeed, the calculated H−H bond distance distribution, as shown in Figs. 1, 2(b), clearly illustrates that all H atoms are well separated by at least 2.1 Å on Pt_4H_{16}, while a peak around 0.75 Å corresponding to a H_2 molecule is observed on Pt_4H_{18}.

For all smaller Pt_n (n = 2–9) clusters, the calculated H_2 dissociative chemisorption energy E_{CE}, H sequential desorption energy E_{DE} and the loss of electrons of metal clusters Q exhibit similar features, as shown in Fig. 2. The general trends of these quantities are that they decline with the H coverage. However, while both E_{CE} and Q decrease monotonically with the number of H atoms, some fluctuation of E_{DE} is observed. This is because H atoms first saturate the energetically most favorable sites. As these sites are filled, their stability decreases and the vacant sites begin to fill. Full H saturation can be identified using MD simulations, which can distinguish the H_2 molecules physisorbed on the clusters. Figure 2 also indicates that in all cases, at the full saturation, the H_2 dissociative chemisorption energy fluctuates in the range between 0.9−1.1 eV, which is 0.2−0.3 eV higher than the experimental value for the H_2 dissociative chemisorption on the Pt(111) surface at zero coverage. Similarly, the calculated threshold H sequential desorption energy varies in a narrow range of 2.45−2.60 eV, slightly smaller than the value for an isolated H atom on the Pt(111) surface reported in a previous study by Papoian [12].

3.2 Hydrogen chemisorption on the Pt_{13} cluster

We next turn to investigate the hydrogen chemisorption on the larger icosahedral Pt_{13} cluster. Similarly, the adsorption energy on the three possible sites is calculated: on-top, edge and hollow sites. The adsorption energies on these sites are calculated to be 1.37, 1.46 and 1.21 eV, respectively. In contrast to the smaller close-packed clusters, the edge site is identified as the most favorable binding site on the icosahedral Pt_{13} cluster, which is in agreement with the recent DFT/GGA results [23]. Many studies have reported that H_2 molecules can readily dissociate on flat Pt surfaces or clusters [12, 17, 24, 25]. Furthermore, the dissociated H atoms have high mobil-

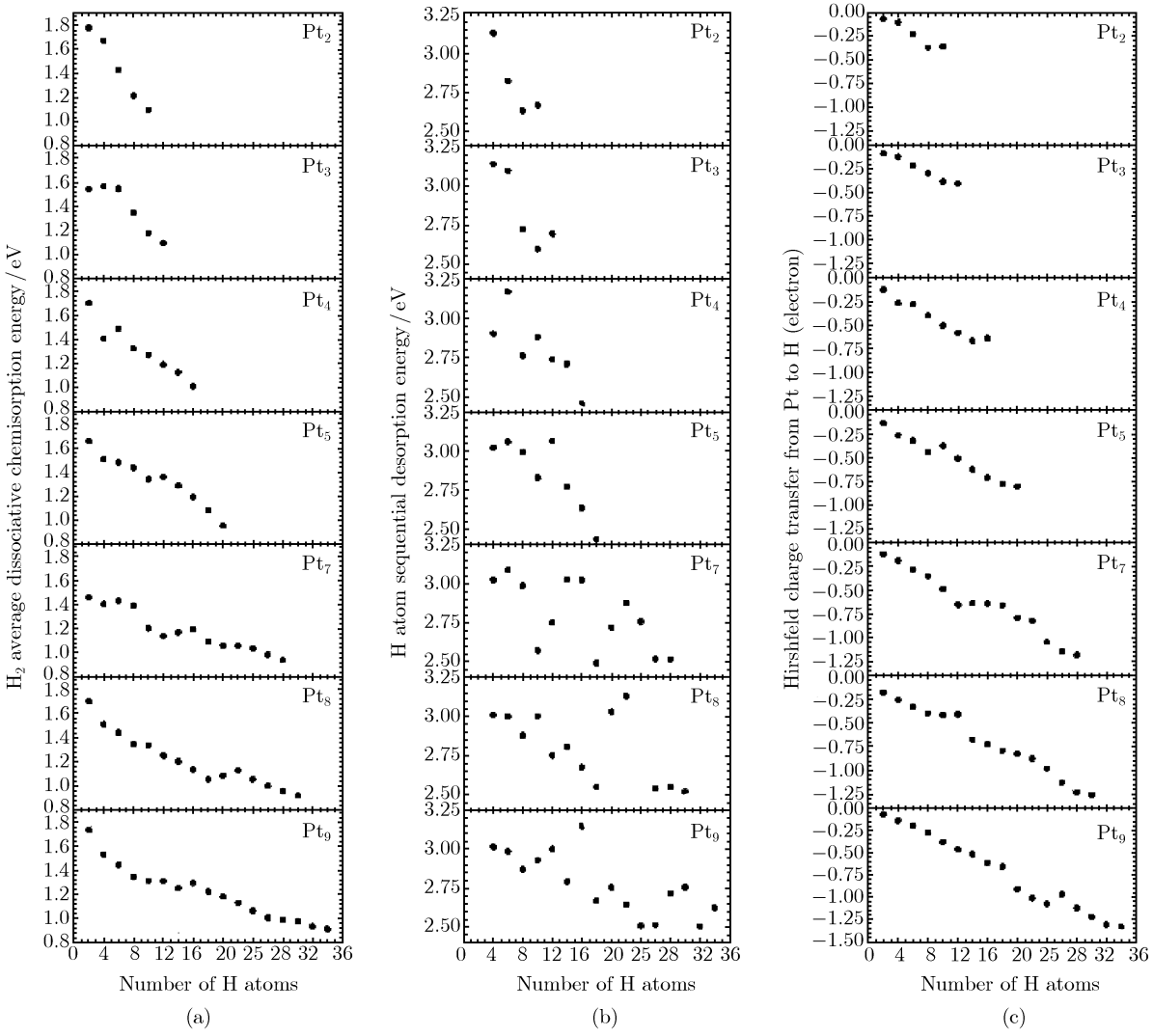

Fig. 2 The calculated **(a)** H_2 dissociative chemisorption energy; **(b)** H desorption energy and **(c)** The loss of Hirshfeld charges of Pt clusters vs. H coverage. Reprinted with permission from Ref. [31]. Copyright © 2007 American Chemical Society.

ity on those surfaces [12, 17]. For comparison, we thus further studied the reaction pathways of H_2 dissociation and H diffusion on the Pt_{13} cluster. Initially, a H_2 molecule was placed 3.01 Å above the on-top site to ensure no chemical bonding between H and Pt atoms, as shown in Fig. 3. The dissociation of H_2 is found to be nearly barrierless (TS1, 0.06 eV), and the subsequent H diffusion barriers are smaller than 0.34 eV. The final product (P3) has a chemisorption energy of 1.65 eV with the two H atoms well separated on the edge sites. Therefore, the H_2dissociation is ready to proceed on the on-top sites, which clearly highlights the catalytic activity of the Pt_{13} cluster. Subsequently, H atoms can readily overcome the moderate activation barriers and migrate from the on-top sites to the more favorable edge sites.

We then sequentially placed more H atoms onto the edge sites of the Pt_{13} cluster and then fully optimized the structures. All the optimized configurations were examined by MD simulations to determine whether the system has reached full H saturation. A few selected structures are displayed in Fig. 4(a). MD simulations and bond distance distribution analysis indicate that the H saturation point on Pt_{13} was located at n=44. Excessive H atoms will recombine to H_2 molecules, resulting in a 0.74 Å peak in the H–H distance distribution, as shown in Fig. 4(b).

Figure 5(a) shows that the average Pt–Pt bond distance increases rapidly with the hydrogen loading at low coverage ($n < 10$), implying that the sequential adsorption of H atoms leads to expansion of the Pt_{13} cluster, which is consistent to the previous reports [4]. However, the icosahedral structure of the Pt_{13} cluster is still maintained and the most stable configurations have symmetric H–H pair distribution until $n = 8$, as shown in Fig. 4(a_2). We thus denote this stage ($n < 10$) as the icosahedron stage. However, the Pt_{13} icosahedron undergoes a transition to an *fcc*-like structure [Fig. 4(a_3)] when more than 8 hydrogen atoms are chemisorbed. To ensure that it is not an artifact, we performed MD simulations for up to 2 ps for $Pt_{13}H_8$ and found that the

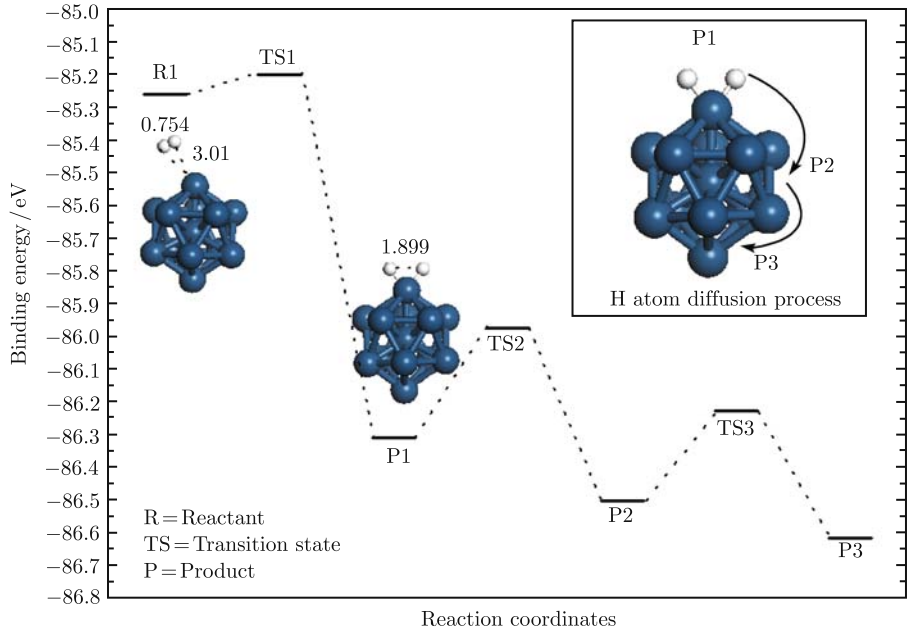

Fig. 3 The H_2 dissociation and H diffusion pathways on the Pt_{13} cluster.

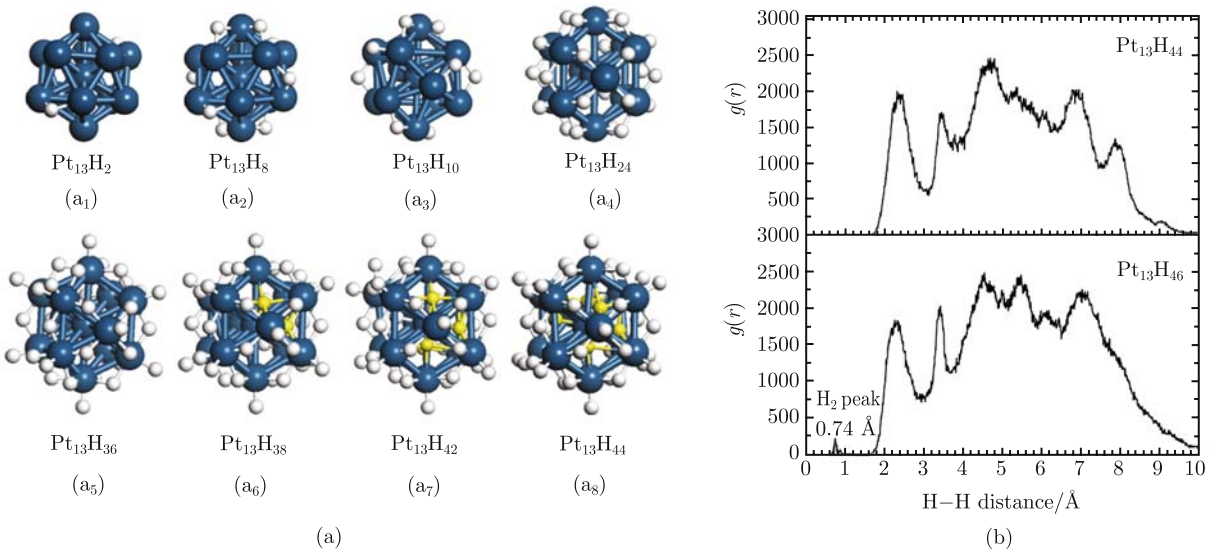

Fig. 4 **(a)** Optimized structures of $Pt_{13}H_n$, the endohedrally adsorbed H atoms are represented as yellow spheres; **(b)** The calculated H−H distance distributions of $Pt_{13}H_{44}$ and $Pt_{13}H_{46}$.

icosahedral structure was stable. We then placed two more H atoms on the vacant edge sites and performed MD simulations for 2 ps again. The energy evolution curve and the average Pt–Pt bond distance change during the MD simulations are shown in Fig. 5(b_1) and (b_2), respectively. At the initial period (500 ps) of the MD simulations, only thermal motion of Pt and H atoms were observed. However, in contrast to $Pt_{13}H_8$, there are four additional Pt−H bonds formed and the Pt–Pt bond strength was weakened. Consequently, the symmetry of the Pt_{13} icosahedron is destroyed and the icosahedron starts to evolve to an *fcc*-like cluster. Indeed, Fig. 5(b) clearly indicates that with an *fcc*-like structure, the $Pt_{13}H_n$ hydride can have a minimum total energy and shortest average Pt–Pt bonds. As shown in Fig. 4(a_4), the *fcc* feature is gradually consummated until the edge sites are all occupied (n=24).

The homogeneously absorbed H atoms at the edge sites are all distributed around the *fcc* Pt_{13} and formed two types of 4-membered H rectangles. One type of the rectangles has a Pt atom in the plane center (denoted as Pt@H_4), while the other type of rectangles has no central Pt atoms, namely, the Vac−H_4 sites. Our calculations indicate that the hydrogen adsorption energy at the

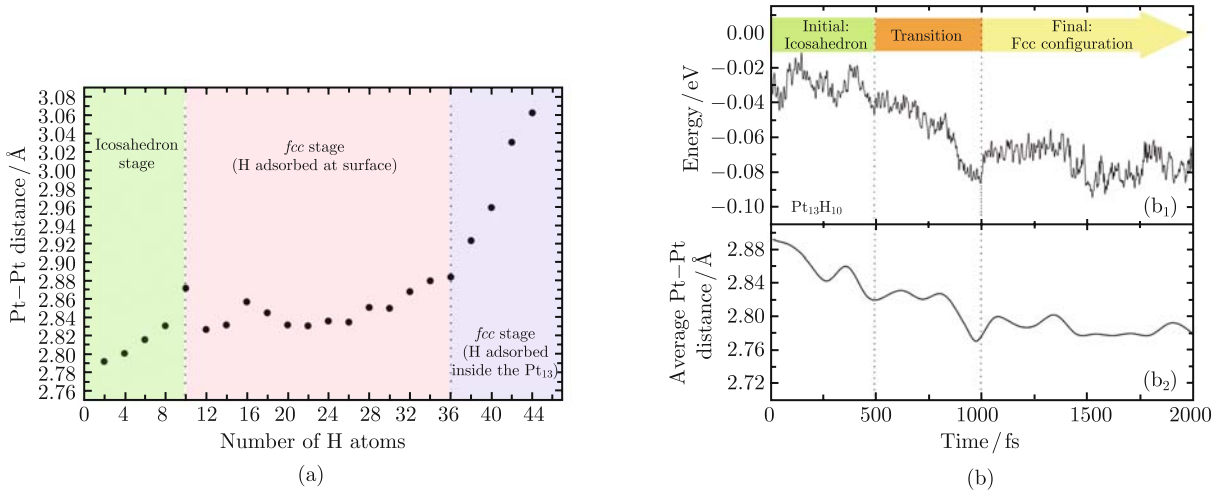

Fig. 5 **(a)** The calculated average Pt–Pt bond distance of $Pt_{13}H_n$; **(b_1)** The total energy of $Pt_{13}H_{10}$ system; **(b_2)** The calculated average Pt–Pt distances of $Pt_{13}H_{10}$ during the MD simulations.

$Pt@H_4$ site is around 0.12 eV higher than the $Vac-H_4$ site, which is calculated to be 1.41 eV. The $Pt@H_4$ were then sequentially filled by up to 12 H atoms until n=36, as shown in Fig. 4(a_5) and the middle part of Fig. 5(a). All the hydrogen atoms were absorbed on the surface of the Pt_{13} cluster and the average Pt–Pt bond lengths fluctuate in a small range of 2.83−2.88Å with the increasing H loading. Additional H atoms placed on the 6 $Vac-H_4$ sites will penetrate into the cluster and interact with the core Pt atom [Fig. 4(a_6)–(a_8)]. Indeed, the endohedrally adsorbed H atoms will significantly weaken the interactions between the core and shell Pt atoms, leading to further expansion of the Pt_{13} structure, as shown in the third stage in Fig. 5(a). Such adsorption behavior of H on the Pt_{13} icosahedral cluster is quite different from the smaller close-packed clusters because those smaller clusters have no inner atoms. However, such phenomena have been observed for H adsorption on the Pt crystalline surfaces where H atom could diffuse into the Pt lattice after all the surface sites are filled [9].

Figure 6 displays the H_2 dissociative chemisorption energies (ΔE_{CE}), the H sequential desorption energies (ΔE_{DE}) and the Hirshfeld charge transfer from Pt_{13} to H atoms (ΔQ) with respect to the H coverage. Before the edge sites were filled up, both ΔE_{CE} and ΔQ curve fluctuates in a very small range of 1.55−1.68 eV and 0.05−0.08 electrons, respectively. Upon the phase transition, when H atoms penetrate into the cluster, ΔE_{CE} and ΔE_{DE} start to drop rapidly to 0.9 eV and 2.02 eV, respectively. Compared to smaller Pt clusters, we can conclude that the phase transition will be beneficial to the catalytic activity of Pt_{13} because the dissociative chemisorption energy of H_2 on those small clusters drops rapidly with the increasing loading. The cluster itself relaxes [Fig. 5(a)] due to the H adsorption, allowing additional H atoms to reside at $Pt@H_4$ and $Vac-H_4$ sites. Compared to the single crystalline surface, the threshold ΔE_{CE} is about 0.2 eV higher, which indicates higher reactivity towards H_2 dissociation. In contrast, the threshold ΔE_{DE} is 0.6 eV lower than on the single crystalline surface, implying that the desorption of H atoms is much easier. In addition, compared to the close-packed small Pt clusters, ΔE_{CE} is almost identical while ΔE_{DE} is slightly lower by about 0.2 eV. Apparently, the vast difference of the sizes and shapes will not change the ΔE_{CE} and ΔE_{DE} significantly.

3.3 Hydrogen chemisorption on close-packed Pd_n clusters (n = 2–9)

We now investigate the H_2 dissociative chemisorption, H sequential desorption on the Pd clusters as well as their structural phase transition. In contrast to the Pt clusters, the edge site was identified as the most favorable binding site for H atoms on both close-packed and icosahedral Pd clusters. Figure 7(a) displays the optimized structures of the fully H saturated Pd_n(n = 2–9) clusters. It is interesting to note that the H capacity of small Pd clusters is roughly half of that of small Pt clusters except for n = 2 and 3. Most of the adsorbed H atoms reside at the edge and hollow sites, while H atoms tend to fill in the on-top sites of the close-packed Pt clusters first. For larger Pd clusters, some of the on-top sites are also populated.

In Fig. 8(a), the calculated sequential dissociative chemisorption energies E_{CE} of H_2 molecules on the Pd_n (n = 2–9) clusters are displayed. In general, the energy decreases as H coverage increases. Furthermore, at low H coverage, the dissociative H_2 chemisorption energies are reduced with cluster size. Except for n=2 and 3, the calculated threshold E_{CE} fluctuates between 0.6−0.9 eV, slightly lower than that of small Pt clusters. For Pd_2H_2,

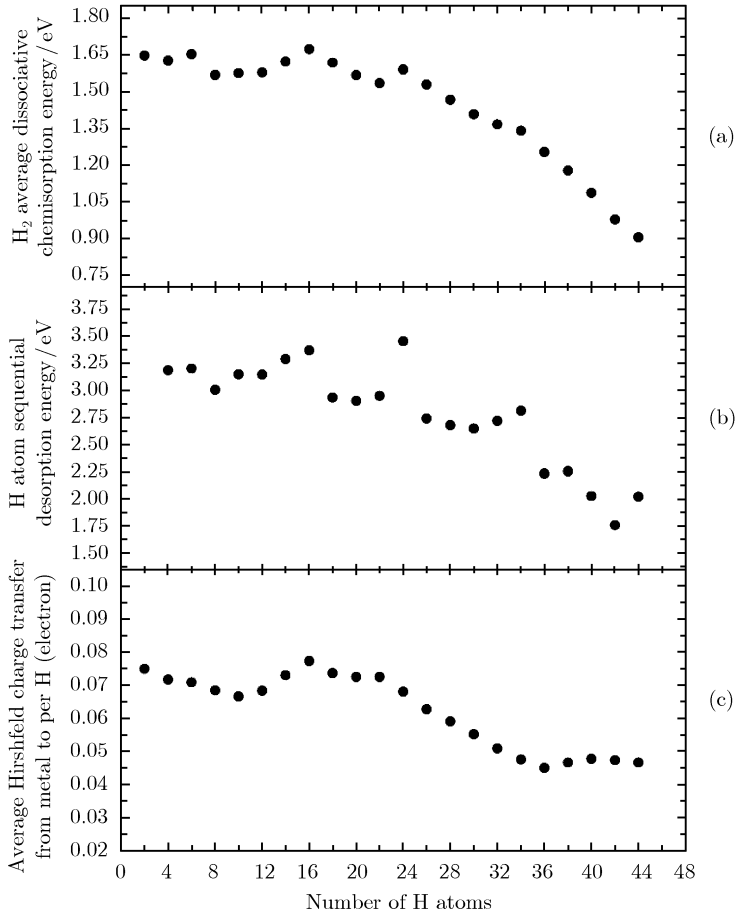

Fig. 6 The calculated **(a)** dissociative chemisorption energy, **(b)** sequential desorption energy and **(c)** Hirshfeld charge transfer from Pt_{13} to H atoms.

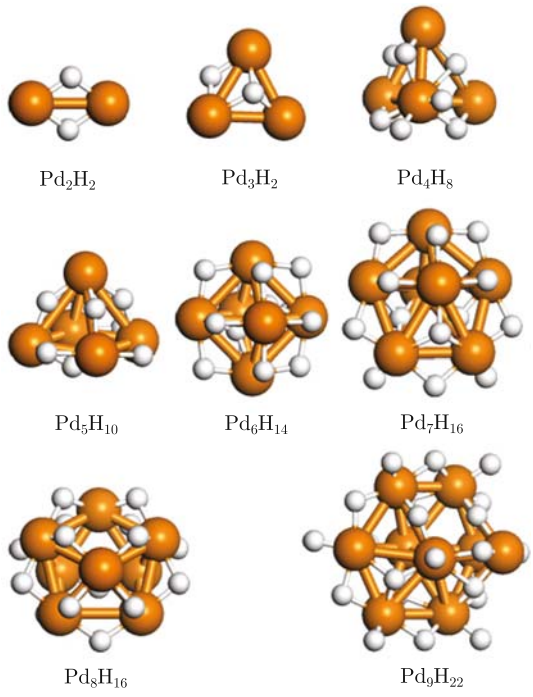

Fig. 7 Optimized structures of fully H saturated Pd_n clusters (n = 2–9). Reprinted with permission from Ref. [32]. Copyright © 2008 The Royal Society of Chemistry.

the surprisingly large E_{CE} value can be attributed to its relatively stable electronic structure. Pd_2 cluster is magnetic with two unpaired electrons. Upon H_2 chemisorption, its electronic structure becomes a close-shell and thus stable. Figure 8(b) shows the calculated sequential desorption energies of H atoms from the Pd clusters. For n=2 and 3, the desorption energies are simply the values of their dissociative chemisorption energies. For larger clusters, the calculated threshold E_{DE} varies in a range of 2.29−2.80 eV, similar to what was found for Pt clusters, which is considerably higher than the value of H desorption on Pd crystalline surface at high coverage. Although the general trend is that E_{DE} decreases with cluster size, there appears some fluctuation in the calculated desorption energies due to the fact that the sequential desorption energy is evaluated from the difference between $E_{Pd_nH_x}$ and $E_{Pd_nH_{x-2}}$ and some of the smaller clusters can be less stable than the larger ones. Figure 8(c) shows the calculated sequential Hirshfeld charges transferred from Pd clusters to H atoms. Similar to small Pt clusters, the Pd clusters donate electron to H atoms and the charge transfer from Pd clusters to H atoms increases monotonically as H coverage increases, leading to hydride formation.

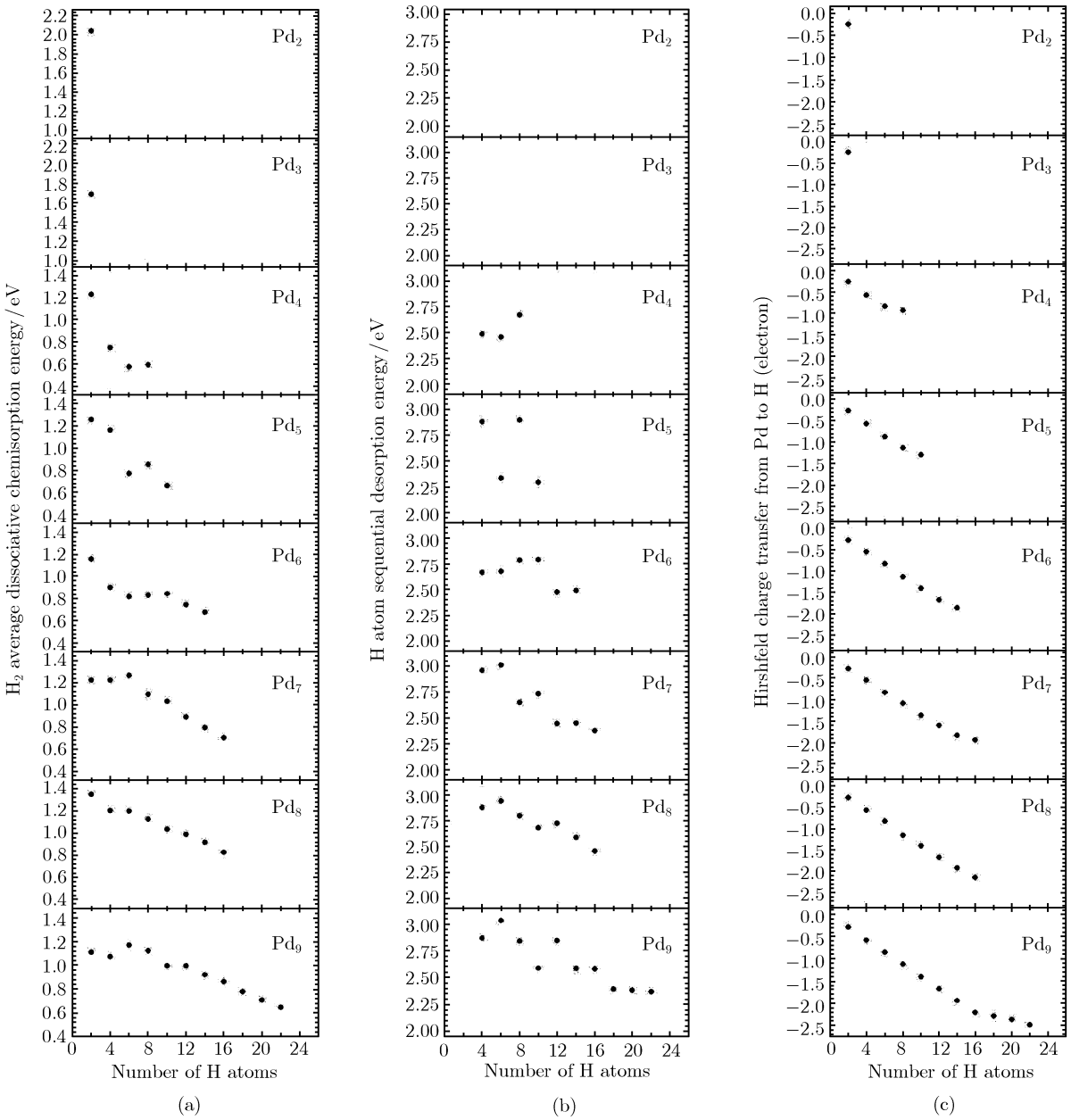

Fig. 8 **(a)** The calculated H_2 dissociative chemisorption energy; **(b)** H desorption energy and **(c)** The loss of Hirshfeld charges of Pd clusters vs. H coverage. Reprinted with permission from Ref. [32]. Copyright © 2008 The Royal Society of Chemistry.

3.4 Hydrogen chemisorption on the Pd_{13} cluster

The calculated H_2 dissociative chemisorption energy on the edge site of the Pd_{13} cluster is 1.40 eV. The H_2 dissociation and H diffusion activation barriers are calculated to be 0.16 eV and 0.07 eV, respectively. Compared to the Pt_{13} cluster, the dissociation of H_2 on Pd_{13} is slightly more difficult, while the H diffusion is much more facile. Sequentially introducing H atoms to the Pd_{13} cluster also leads to the phase transition from the icosahedral to *fcc*-like structures. A few selected $Pd_{13}H_n$ hydride structures are displayed in Fig. 9. The phase transition point is located at n=20 and the transformation consummates at n=24 where all the edge sites are filled. Unlike the Pt_{13} cluster, the two additional H atoms introduced to the $Pd_{13}H_{24}$ hydride would be pulled into the cluster and interact with the core Pd atom instead of staying on the surface. However, the Pd_{13} cluster can hold only 2 H atoms inside, while the Pt_{13} cluster can accommodate 6 H atoms inside. The H desorption energy on Pd_{13} is lower than on Pt_{13}. Consequently, H atoms would be much easier to desorb from Pd than Pt clusters, implying that Pt clusters may have a much higher hydrogen sorption capacity. Indeed, upon full H saturation, the Pd_{13} cluster can only hold around 2/3 of the amount of H atoms that the Pt_{13} cluster can hold. Additional H atoms placed on the $Pd_{13}H_{26}$ hydride will not penetrate

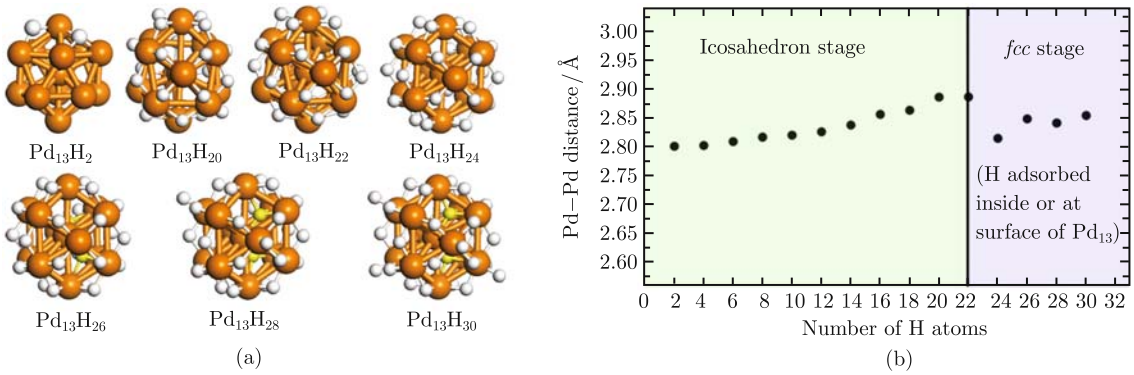

Fig. 9 **(a)** Optimized structures of $Pt_{13}H_n$; **(b)** The calculated average Pd−Pd bond lengths of $Pd_{13}H_n$.

into the cluster but absorb at the Pd@H_4 corner sites instead. The saturation point identified by MD simulation is located at $n = 30$.

The calculated H_2 threshold dissociative chemisorption energy and H desorption energy at full saturation are 0.76 eV and 2.04 eV [Fig. 10(a) and (b)], comparable to those values on smaller close-packed Pd clusters. Therefore, we believe that, these two important properties, ΔE_{CE} and ΔE_{DE}, do not vary with sizes and shapes for both Pt and Pd clusters with up to 13 atoms. The main factor that controls the catalytic properties towards H_2 dissociative chemisorption is how many Pt or Pd atoms can be accessed by H_2 molecules. As shown in Fig. 10(c), the loss of electrons ΔQ from metal cluster to average per H atom drops almost linearly with the increasing H loading. We also note that charge transfer

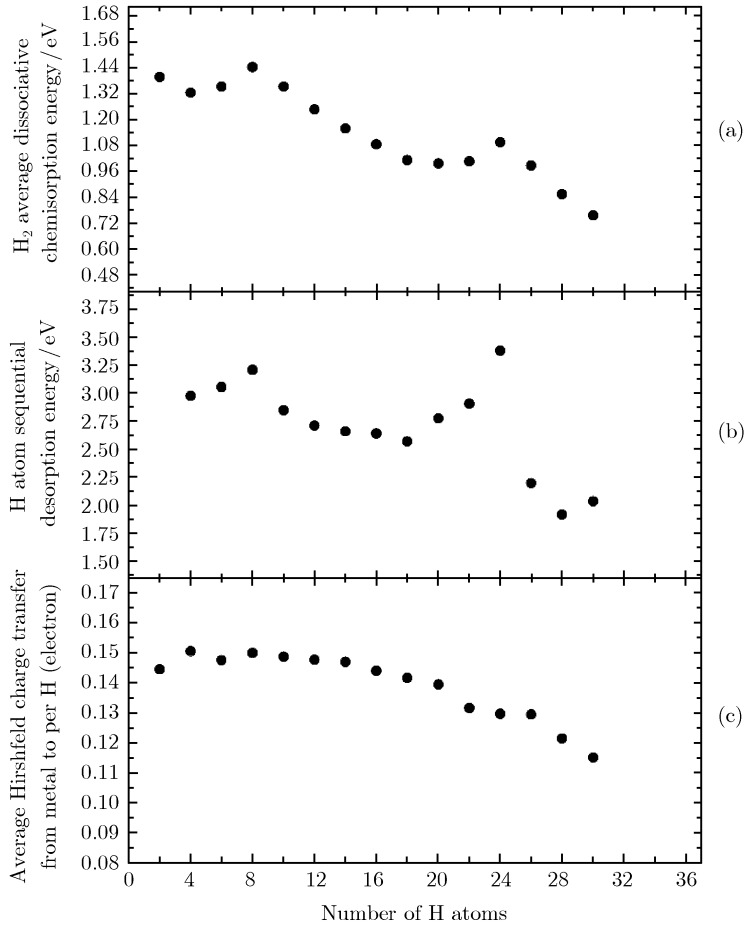

Fig. 10 The calculated **(a)** dissociative chemisorption energy, **(b)** sequential desorption energy and **(c)** Hirshfeld charge transfer from Pd_{13} to H atoms.

of $Pd_{13}H_n$ hydride is much higher than that of $Pt_{13}H_n$.

3.5 Electronic properties

Figure 11 displays the calculated density of states (DOS) of both bare and fully saturated Pt_{13} and Pd_{13} clusters. Upon H_2 adsorption on Pt_{13} and Pd_{13} clusters, hydrogen coverage alters the electron spin density of the cluster surface, which affects the electronic properties of catalysts. Our calculations indicate that the bare clusters exhibit certain magnetic moments. Upon full saturation by H atoms, the Pt and Pd hydrides exhibit close-shell features due to the fact that the unpaired Pd/Pt-d electrons will interact with the H-1s orbital, which annihilates the magnetic moments. Detailed analysis shows that the valence bands are contributed mostly by the d-orbitals of metal atoms and the s-orbitals of H atoms. The conduction bands are mostly contributed by the 5d- and 6s-orbitals of Pt atoms, while 4d-and 5s-orbitals of Pd atoms. Since the interaction between H-1s and Pt-5s is stronger than the interaction between H-1s and Pd-4d, the band gap of $Pt_{13}H_{44}$ is smaller than that of $Pd_{13}H_{30}$.

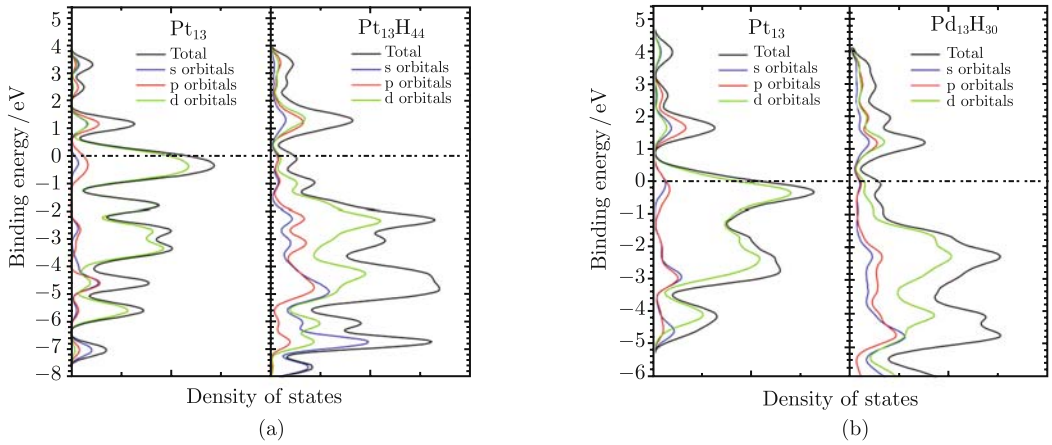

Fig. 11 The calculated density of states of **(a)** bare Pt_{13} cluster and H saturated Pt_{13} cluster; **(b)** bare Pd_{13} cluster and H saturated Pd_{13} cluster.

4 Conclusions

Pt and Pd clusters catalyzed hydrogenation reactions play a very important role in many applications and industrial processes and thus have initiated intensive theoretical and experimental studies. In this review, we summarize our recent studies that attempted to quantitatively address the catalytic performance of small Pt and Pd clusters toward H_2 chemisorption and H desorption using first principles methods. We chose several close-packed Pt_n and Pd_n ($n = 2$–9) clusters, as well as icosahedral Pt_{13} and Pd_{13} clusters to systematically investigate the size/shape effects on the sequential H_2 dissociative chemisorption and H desorption. For both Pt_{13} and Pd_{13}, their H_2dissociative chemisorption energy and H desorption energy at full saturation are comparable to what were calculated for smaller close-packed clusters. This clearly suggests that some important properties related to the catalytic performance of transition metal clusters may not vary significantly with the particle size or shape. However, these properties are dependent on the available surface metal atoms that can be accessed by H atoms. In addition, our study indicates that Pt clusters have a much higher hydrogen adsorption capacity than Pd clusters. We are also aware that our calculations are based on the Pt and Pd clusters with no more than 13 atoms. Hence, our conclusions are probably limited to the subnano clusters. Further studies on larger-scale clusters are required to enhance our understanding of the size-dependency of metal catalytic performance.

Acknowledgements This work was supported by the National Natural Science Foundation of China (Grant No. 10844001) and the Natural Science Foundation of Zhejiang Province (Grant No. Y7080425).

References

1. B. C. H. Steele, Nature (London), 1999, 400: 619
2. S. F. Parker, C. D. Frost, M. Telling, P. Albers, M. Lopez, and K. Seitz, Catal. Today, 2006, 114: 418
3. P. S. Cremer, X. Su, Y. R. Shen, and G. A. Somorjai, J. Am. Chem. Soc., 1996, 118: 2942
4. Y. Li and R. T. Yang, J. Am. Chem. Soc., 2006, 128: 726
5. Y. Li and R. T. Yang, J. Am. Chem. Soc., 2006, 128: 8136
6. T. E. Felter, S. M. Foiles, M. S. Daw, and R. H. Stulen, Surf. Sci. Lett., 1986, 171: 379
7. S. Horch, H. T. Lorensen, S. Helveg, E. Lægsgaard, I. Stensgaard, W. Jacobsen, J. K. Nøskov, and F. Besenbacher, Nature (London), 1999, 398: 134

8. S. C. Badescu, P. Salo, T. Ala-Nissila, S. C. Ying, K. Jacobi, Y. Wang, K. Bedurftig, and G. Ertl, Phys. Rev. Lett., 2002, 88: 136101
9. P. Légaré, Surf. Sci., 2004, 559: 169
10. M. K. Oudenhuijzen, J. A. Bokhoven, J. T. Miller, D. E. Ramaker, and D. C. Koningsberger, J. Am. Chem. Soc., 2005, 127: 1530
11. X. Liu, H. Dilger, R. A., R. A. Eichel, J. Kunstmann, and E. Roduner, J. Phys. Chem. B, 2006, 110: 2013
12. G. Papoian, J. K. Nøskov, and R. Hoffmann, J. Am. Chem. Soc., 2000, 122: 4129
13. D. Godbey and G. A. Somorjai, Surf. Sci., 1988, 204: 301
14. K. Christmann, Surf. Sci. Rep., 1988, 9: 1
15. B. Hammer and J. K. Nøskov, Nature (London), 1995, 376: 238
16. R. A. Olsen, G. J. Kroes, and E. J. Baerends, J. Chem. Phys., 1999, 111: 11155
17. G. W. Watson, R. P. K. Wells, D. J. Willock, and G. J. Hutchings, J. Phys. Chem. B, 2001, 105: 4889
18. K. Nobuhara, H. Kasai, W. Q. Dino, and H. Nakanishi, Surf. Sci., 2004, 566–568: 703
19. K. Nobuhara, H. Kasai, H. Nakanishi, and A. Okiji, J. Appl. Phys., 2002, 92: 5704
20. L. Barrio, P. Liu, J. A. Rodriguez, J. M. Campos-Martin, and J. Fierro, J. Chem. Phys., 2006, 125: 164715
21. Z. P. Liu and P. Hu, J. Am. Chem. Soc., 2003, 125: 1958
22. X. Q. Gong, A. Selloni, O. Dulub, P. Jacobson, and U. Diebold, J. Am. Chem. Soc., 2008, 130: 370
23. X. Liu, H. Dilger, R. A. Eichel, J. Kunstmann, and E. Roduner, J. Phys. Chem. B, 2006, 110: 2013
24. Y. Okamoto, Chem. Phys. Lett., 2006, 429: 209
25. Y. Okamoto, Chem. Phys. Lett., 2005, 405: 79
26. G. E. Gdowski, J. A. Fair, and R. J. Madix, Surf. Sci., 1983, 127: 541
27. L. J. Richter and W. Ho, Phys. Rev. B, 1987, 36: 9797
28. C. T. Au, T. J. Zhou, and W. J. Lai, Catal. Lett., 1999, 62: 147
29. N. Watari and S. Ohnishi, J. Chem. Phys., 1997, 106: 1997
30. L. Chen, A. C. Cooper, G. P. Pez, and H. Cheng, J. Phys. Chem. C, 2007, 111: 5514
31. C. Zhou, J. Wu, A. Nie, R. C. Forrey, A. Tachibana, and H. Cheng, J. Phys. Chem. C, 2007, 111: 12773
32. C. Zhou, S. Yao, J. Wu, R. Forrey, L. Chen, A. Tachibana, and H. Cheng, Phys. Chem. Chem. Phys., 2008, 10: 5445
33. W. Dong and J. Hafner, Phys. Rev. B, 1997, 56: 15396
34. J. P. Perdew and Y. Wang, Phys. Rev. B, 1992, 45: 13244
35. T. A. Halgren and W. N. Lipscomb, Chem. Phys. Lett., 1977, 49: 225
36. F. L. Hirshfeld, Theor. Chim. Acta B, 1977, 44: 129
37. B. Delley, J. Chem. Phys., 2000, 113: 7756
38. B. Delley, J. Chem. Phys., 1990, 92: 508
39. A. Nie, J. Wu, C. Zhou, S. Yao, C. Luo, R. C. Forrey, and H. Cheng, Int. J. Quantum Chem., 2007, 107: 219